Engineered 2D PbX (X = S, Se, Te) Monochalcogenides: Pressure-Tuned Optoelectronic Properties for Deep-Space Photovoltaics

M. Tariq[1,2,*], R. Ahmed[1,2], S. A. Tahir[1], B. U. Haq[3], F. K. Butt[4], M. W. Majeed[1] and A. Hussain[1]

[1]NRPU Lab, Centre for High Energy Physics, University of the Punjab Quaid-e-Azam Campus, University of the Punjab Lahore, Lahore, 54590, Pakistan
[2]Department of Physics, Faculty of Science, Universiti Teknologi Malaysia, Johor Bahru, 81310, Malaysia
[3]Department of Mechanical Engineering, College of Engineering, Prince Mohammad Bin Fahd University, Alkhobar, 31952, Saudi Arabia
[4]Department of Physics, Division of Science and Technology, University of Education Lahore, Lahore, 54770, Pakistan
*Corresponding Author: M. Tariq. Email: tariq1981@graduate.utm.my or tariqphy109@gmail.com
Received: 13 October 2025; Accepted: 11 December 2025

ABSTRACT: The two-dimensional IV-monochalcogenides, such as lead sulfide (PbS), lead selenide (PbSe), and lead telluride (PbTe), represent a promising class of materials known for their remarkable optoelectronic properties. The calculated binding energies for the puckered phase were −4.25 eV for PbS, −4.20 eV for PbSe, and −3.02 eV for PbTe, indicating strong stability in PbS and PbSe compared to PbTe. The electronic analysis showed that PbS exhibited a band gap of 1.01 eV, while PbSe had a slightly lower band gap of 0.70 eV. Under applied pressure, both materials demonstrated an increase in band gap, rising to 1.90 eV for PbS and 1.32 eV for PbSe, suggesting enhanced semiconducting behavior. In contrast, PbTe displayed non-monotonic behavior in its band gap variation with pressure, reflecting its complex electronic structure. Overall, PbS showed excellent potential for boosting solar cell efficiency, while PbSe confirmed its promise for advanced photovoltaic device applications.

KEYWORDS: DFT; 2D IV-monochalcogenides; structural properties; electronic band gap

1 Introduction

Space exploration has been entered in a new phase, with emissions focusing on more hostile and severe environmental conditions such as frozen moons, underground oceans, and planet depths [1]. A major challenge is ensuring a consistent energy source for long-term operations in these conditions. Traditional photovoltaic systems, which operate well on Earth, are limited when used on planets with strong atmosphere pressure and geological forces, such as Mars, or frozen moons like Europa [2]. Europa's subsurface oceans, for example, experience pressures exceeding 100 mega Pascal (MPa), about 1000 times Earth's sea level pressure [3]. Under such conditions, traditional Silicon-based solar cells [4], which are heavy and rigid, or organic solar cells [5], which suffer lower efficiency and stability, perform poorly. Even high-efficiency perovskite solar cells [4] and copper indium gallium selenide (CIGS) solar cells [6,7] face challenges, such as manufacturing scalability, fluctuating efficiency, and durability concerns [4] under these intense conditions. As a result, there is a pressing need for new solar materials that are affordable, lightweight, flexible, and highly efficient under high pressure.

The IV-monochalcogenides have attracted strong attention for their application as for solar cells materials, particular in space technology. Numerous theoretical studies [8–10] have demonstrated that two-dimensional IV-monochalcogenides exhibit unique combination of properties, making them attractive candidates for advanced solar cells and optoelectronic technologies in space. For instance, Xu and colleagues [10] used density-functional theory and many-body perturbation theory to explore the electronic and optical properties of monolayer group-IV monochalcogenides (MX), where M = Ge, Sn and X = S, Se, Te. Their analysis revealed that the estimated carrier mobility, ranging from 10^3 to

https://doi.org/10.15251/CL.2025.2212.1067

10^5 cm^2 V^{-1} s^{-1}, rival those of phosphorene, as modeled through phonon-limited scattering. This mobility makes them well-suited for optoelectronics applications. DFT calculations performed by Xu et al. [10] revealed that GeSe monolayers possess a direct band gap of 1.66 eV, making them highly suitable for optoelectronic applications. Similarly, Peng et al. [11] conducted first-principles simulations to investigate the electronic properties of SnS and SnSe monolayers, providing insights into their potential use in advanced electronic devices. Furthermore, Dai et al. [12] utilized *ab initio* molecular dynamics (AIMD) to study a series of IV–VI monochalcogenide monolayers, including GeS, GeSe, GeTe, SnS, and SnTe. Their calculated band gaps were 3.27 eV for GeS, 3.00 eV for GeSe, 2.38 eV for GeTe, 2.87 eV for SnS, and 2.46 eV for SnTe, demonstrating a broad range of electronic tunability among these materials. Despite these promising characteristics and their potential for photovoltaic applications, subsequent studies [13] highlighted that several challenges remain in optimizing their performance for practical device implementation.These include limitations in efficiency, scalability in manufacturing, and concerns regarding long-term stability under environmental conditions. Specifically, Sn-based materials may struggle with low absorption coefficients and poor carrier mobility, while Ge-based materials issues related to high cost and limited availability.

Lead sulfide (PbS) [14], lead Selenide (PbSe) [15], and lead telluride (PbTe) [16], also part of the two-dimensional IV-monochalcogenide family, have sparked considerable attention due to their promising applications in solar energy. Multiple theoretical studies [17–20] have shown the properties found in PbS, PbSe, and PbTe, making them suitable for solar cells and optoelectronic technology [20]. Significant research has been devoted to exploring the features of PbS, PbSe, and PbTe. Boukharis et al. [21] investigated the structural properties of PbS, PbSe, and PbTe using the full-potential linear augmented plane wave (FP-LAPW) method. In an experimental study, Stewart et al. [16] examined p-type PbTe as an ohmic contact to CdTe, PbS and PbSe in particular, offer excellent performance with their adjustable band gaps. Time-resolved photoluminescence measurements indicated significant improvements in photocarrier lifetime, leading to enhanced power conversion efficiency, primarily due to an increased fill factor [18]. Haq et al. [22] found that monolayers of lead-chalcogenides (PbX, X = S, Se, T) demonstrated improved thermoelectric performance at room temperature, especially for PbTe, indicating promise for nanoscale thermoelectric applications. Ye et al. [13] employed density functional theory (DFT) calculations combined with optical analysis to investigate few-layer PbSe sheets. Their study revealed a blue-shifted band gap resulting from quantum confinement effects, leading to an enhanced and advantageous optical band gap.

Furthermore, studies [23–26] have highlighted the significant influence of external pressure on the electronic properties of two-dimensional chalcogenide materials. In [23], the application of external pressure to two-dimensional transition metal chalcogenides enabled precise tuning of their electronic band gaps, demonstrating pressure as an effective tool for modifying material properties. Similarly, investigations in references [24,25] on 2D monochalcogenides revealed a pressure-induced transition from semiconducting to metallic behavior, indicating the potential for phase and property control through external stress. Moreover, Sohrabikia et al. [20] explored PbS and PbSe monochalcogenides under varying pressure conditions and observed a significant non-linear change in their band gaps. These findings suggest that pressure modulation can be strategically employed to optimize material properties for advanced energy and space technology applications.

This research work highlights a clear and robust link between applied stress and the changes observed in their structural, and electronic properties PbS, PbSe, and PbTe [20]. The impact of varying pressure on the 2D PbS, PbSe, and PbTe in puckered structure is rarely reported, hence leaving room for further exploration, particularly for space technology applications.

Building on these compelling discussions for 2D monolayers PbS, PbSe, and PbTe under varying pressure conditions underscores the importance of conducting further investigations into their behavior, particularly in high-pressure environments, to achieve a more comprehensive understanding of their properties. Therefore, this work aims to examine the electronic and optical properties of two-

dimensional IV-monochalcogenides PbS, PbSe, and PbTe under increasing pressure, utilizing DFT calculations to enhance the efficiency for solar cells in space technology.

2 Computational Details

The computational work was performed using the Cambridge Serial Total Energy Package (CASTEP) [26-28]. First-principles calculations based on Density Functional Theory (DFT) were employed, utilizing ultra-soft pseudopotentials for accurate electronic structure representation. The relativistic effects were treated using the Koelling-Harmon approach, while the exchange-correlation interactions were described by the Generalized Gradient Approximation (GGA) with the Perdew–Burke–Ernzerhof (PBE) functional [29]. Geometry optimization was carried out to relieve external stress in the system [30]. The convergence criteria were set such that the Hellmann–Feynman forces were less than 0.03 eV/Å, and the total energy change was below 1×10^{-5} eV. The overall calculation quality was defined as "medium" in the CASTEP settings, with a plane-wave cut-off energy of 489 eV and a self-consistent field (SCF) accuracy of 1×10^{-6} eV

The structural configurations of PbS, PbSe, and PbTe were modeled in three distinct geometries: puckered, buckled, and planar structures as shown in Figure 1. For the puckered configuration, all three materials (PbS, PbSe, PbTe) were constructed following methodologies detailed in Refs. [31], while the buckled structures were developed based on Ref. [31,32]. The planar structures for these materials were generated using parameters from Ref. [33]. Computational setups included a 22 Å vacuum layer to minimize interlayer interactions and a 4 × 4 × 1 supercell to ensure adequate representation of periodic boundary conditions, consistent across all configurations. This systematic approach facilitates comparative analysis of structural properties across different geometries.

The binding energy (B.E.) for puckered, buckled, and planar phases of PbX (X = S, Se, Te) monolayers was uniformly calculated using the formula,

$$B.E = E_{PbX2D} - n[E_{Pb(atom)} - E_{X(atom)}] \quad (1)$$

E_{PbX2D} represents the total energy of the PbX monolayer, n denotes the number of atoms in the unit cell, and $E_{Pb(atom)}$, $E_{X(atom)}$ correspond to the energies of isolated Pb and X atoms, respectively. The thermodynamic stability of each phase was determined by comparing binding energies across configurations, with the lowest B.E. identifying the most stable structure. Dynamic stability was rigorously assessed through phonon dispersion analysis, requiring the absence of imaginary frequencies in the spectra to confirm structural integrity. This dual evaluation, thermodynamic stability via energy minimization and dynamic stability via vibrational robustness, ensured a comprehensive validation of the PbX monolayers' viability. The consistent methodology across all phases enabled systematic comparisons, highlighting the interplay between structural geometry and stability in these 2D systems.

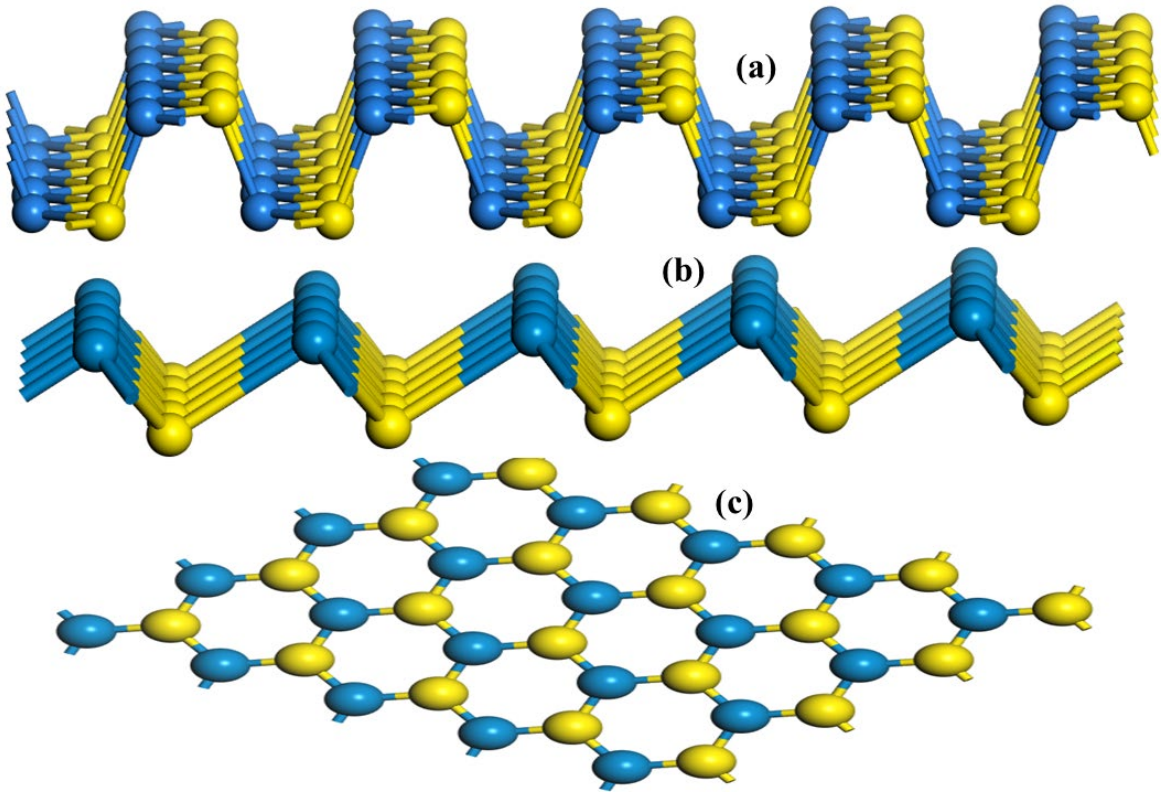

Figure 1: Schematics of 2D Pb-monochalcogenides (PbX; X= S, Se, Te), (**a**) puckered along armchair, (**b**) buckled, and (**c**) planar forms.

3 Results and Discussion

3.1 Structural Stability

Fig. 2 shows that structural and energetic properties of PbX (X = S, Se, Te) monolayers across three phases, puckered (Pmna21), buckled (P3m1), and planar (P6m2), revealing notable trends and are in good agreement with reported values [30,31]. The structural behavior of puckered, buckled, and planar phases reveals distinct trends in lattice constants, bond lengths, and binding energies, as illustrated in Fig. 2a, Fig. 2b, and Fig. 2c, respectively.

The puckered phase is characterized by anisotropic lattice parameters ($a \neq b$), especially for ligh ter chalcogens like S and Se, which exhibit a more pronounced rectangular distortion. For instance, PbS in the puckered form shows a = 3.735 Å and b = 4.88 Å, whereas PbTe displays nearly square symmetry with $a = b$ = 4.61 Å. This contrasts with the buckled phase, which maintains isotropic lattice constants ($a = b$) but with smaller values overall; notably, PbTe in this configuration has a reduced constant of 3.284 Å, deviating from the general increasing trend with chalcogen size. The planar phase presents the largest isotropic lattice constants across all chalcogenides, reaching up to 5.36 Å for PbTe, indicating substantial in-plane expansion due to its flat geometry.

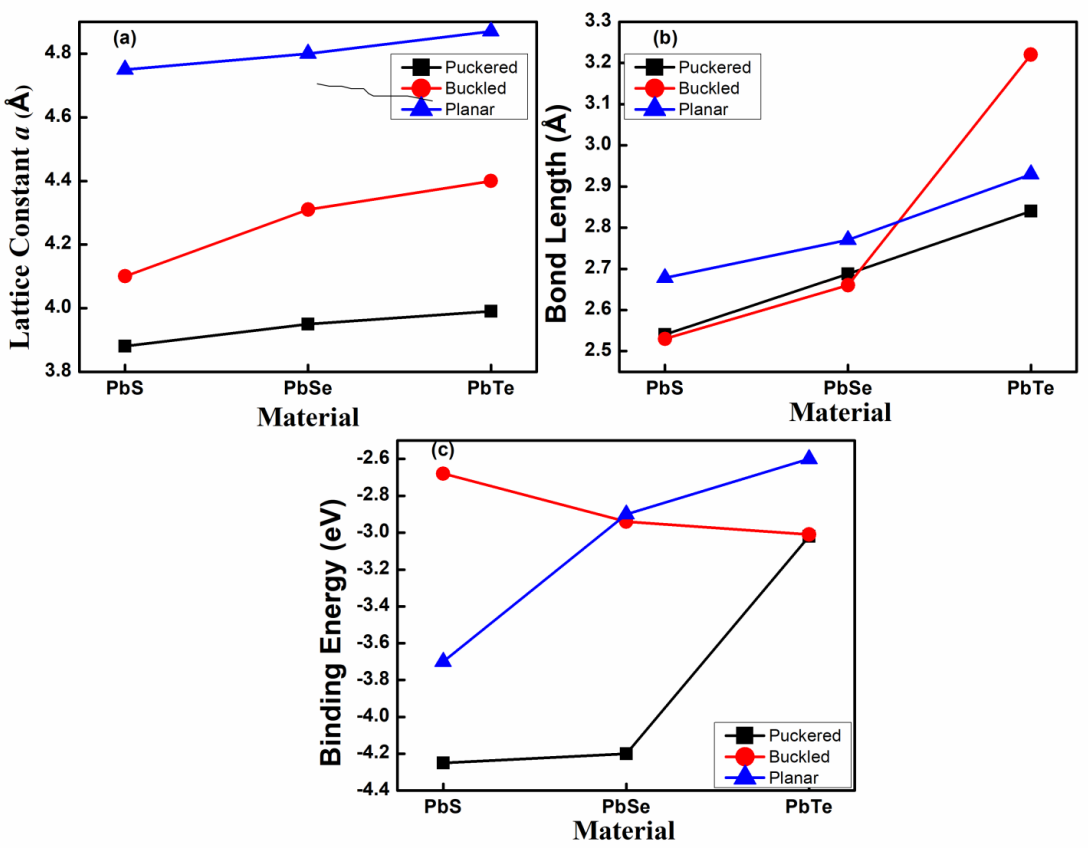

Figure 2: Calculted (**a**) lattice constant a, (**b**) bond lengths, and (**c**) binding energies of 2D Pb-monochalcogenides (PbX; X = S, Se, Te) in puckered, buckled, and planar phases.

As depicted in Fig. 2b, the bond lengths further distinguish these phases. The puckered structure provides the shortest average bond lengths, particularly for PbS (2.54 Å) and PbSe (2.688 Å), signifying stronger covalent bonding driven by the corrugated atomic arrangement. In contrast, the buckled phase shows more variable bond lengths. While PbS (2.53 Å) and PbSe (2.66 Å) in the buckled phase are comparable to their puckered counterparts, PbTe exhibits a significantly elongated bond length of 3.22 Å, likely due to the increased separation induced by out-of-plane buckling. The planar structures consistently show longer bond lengths than the puckered forms; for instance, planar PbS has a bond length of 2.678 Å, implying weaker orbital overlap due to the flattened atomic arrangement.

The binding energy data, shown in Fig. 2c, reflect the relative thermodynamic stability of each phase. The puckered configuration proves most stable for lighter chalcogens, with PbS and PbSe showing high negative binding energies of −4.25 eV and −4.20 eV, respectively. This is attributed to favorable directional bonding and strain relief in their anisotropic geometries. However, the stability of puckered PbTe decreases to −3.02 eV due to less effective bonding. Interestingly, the buckled phase is less stable than the puckered phase for PbS and PbSe (with values of −2.68 eV and −2.94 eV), but it becomes nearly as stable as the puckered form for PbTe (−3.01 eV), indicating that the structural flexibility of the buckled configuration can better accommodate the larger Te atoms. Planar phases fall in between, showing intermediate stability (PbS: −3.90 eV; PbSe: −2.90 eV; PbTe: −2.60 eV), though their flatness may introduce undercoordinated sites or electronic delocalization that slightly weakens bonding. Overall, these results underscore a clear size and phase-dependent trend, where puckered phases dominate for small chalcogens, buckled phases adapt better to larger atoms, and

planar phases, while least stable, might still hold promise due to their symmetry-driven electronic properties.

3.2 Electronic Band Structure

The electronic properties of two-dimensional lead chalcogenide monolayers were analyzed using the GGA (PBE) approach under progressively increasing pressure conditions [34]. The 2D PbS monolayer exhibited an indirect band gap of 1.01 eV, with the valence band maximum (VBM) located at the X-point and the conduction band minimum (CBM) at the Y-point. This value was found to be greater than the 0.23 eV band gap of the three-dimensional PbS–NaCl structure [19], as shown in Fig. 3a. Similarly, the 2D PbSe monolayer showed an indirect band gap of 0.70 eV, where both the VBM and CBM were situated at the X-point, closely matching previously reported data [19], as illustrated in Fig. 3b. In contrast, the 2D PbTe monolayer displayed metallic behavior with no observable band gap, as presented in Fig. 3c. Overall, the applied analysis method effectively characterized the Fermi surface shape and revealed distinct electronic transitions among the PbS, PbSe, and PbTe monolayers [20].

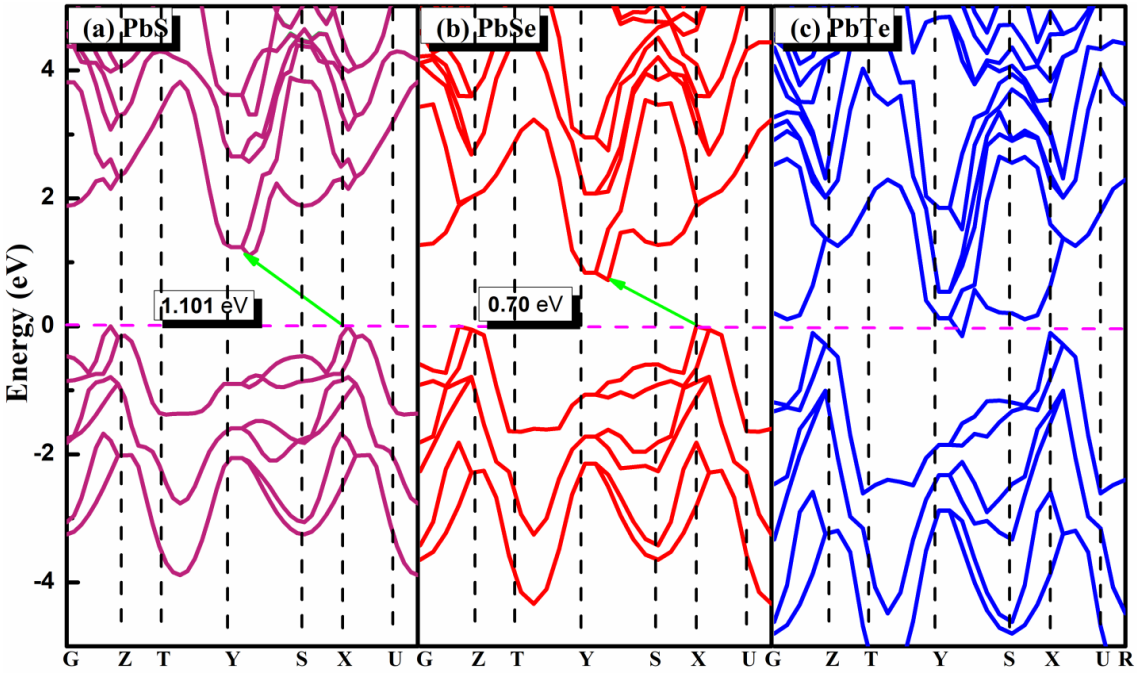

Figure 3: The calculated band structure of 2D-monochalcogenides (**a**) PbS, (**b**) PbSe, (**c**) PbTe.

The band structure of PbS material under increasing pressure is presented in Fig. 4, which shows that a significant upsurge in electronic band gap occurs as pressure varies from 0 to 50 GPa. The band gap experiences a sharp increase from 1.188 eV at 5 GPa to 1.904 eV at 50 GPa. The observed increase in the band gap with pressure is likely due to the heightened effective potential experienced by electrons, caused by closer interlayer spacing and larger atomic constants, which necessitates greater energy for electrons to move from the valence band to the conduction band. Furthermore, the application of pressure compresses the electronic wave functions, resulting in a notable change to electron density distribution with decrease in state overlap and, consequently increased band gap. Prior DFT analyses have reported an enhancement in the band gap of $KBNO_3$ with increasing pressure [35]. Additionally, atomic orbital interactions played a crucial role, as pressure directly impacted the s–p orbital splitting and reduced the p–p orbital overlap. This alteration increased the energy separation

between the conduction band (CB) and the valence band (VB), resulting in a larger band gap. Secondly, the exciton binding energy was enhanced under pressure due to stronger Coulomb interactions between ions, which further contributed to the band gap increase. Lastly, pressure reduced the effective width of the quantum well, thereby intensifying the quantum confinement effect. This enhanced confinement led to an additional increase in the band gap, highlighting the combined influence of orbital interactions, excitonic effects, and confinement on the pressure-dependent electronic properties of the material.

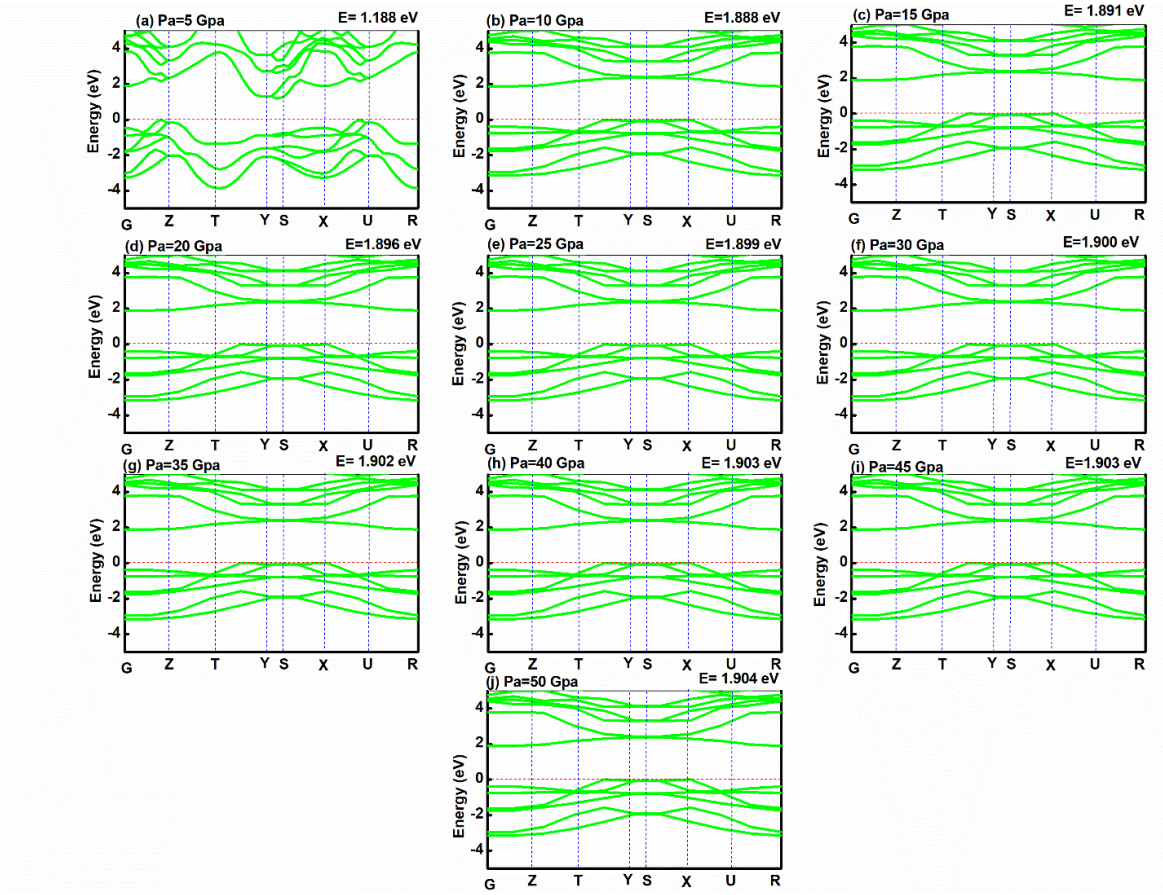

Figure 4: The calculated band structure of 2D-monochalcogenides PbS under varying pressure from 0 to 50 GPa. Subfigures (a) through (j) correspond to the band structures at specific pressure points: (a) 0 GPa, (b) 5 GPa, (c) 10 GPa, (d) 15 GPa, (e) 20 GPa, (f) 25 GPa, (g) 30 GPa, (h) 35 GPa, (i) 40 GPa, and (j) 50 GPa. The progressive changes illustrate the pressure-induced modifications to the band gap and electronic dispersion, potentially indicating a topological phase transition or a direct-to-indirect band gap crossover. The Fermi level is set at 0 eV.

At 0 GPa, PbSe has a band gap of 0.70 eV, as shown in Fig. 5a. As pressure rises, the band gap increases steadily, reaching 1.325 eV at 50 GPa. An identical inverse behavior between an energy gap of 2D-WSe_2 and applied pressure was reported by Shen et al. [25] by using the DFT approach. This gradual upsurge indicates that higher pressure strengthens bonding interactions, leading to a wider band gap. The increased band gap with increasing pressure can be attributed to multiple factors. The applied pressure may shift energy levels within the conduction band, pushing these states higher and widening the band gap.

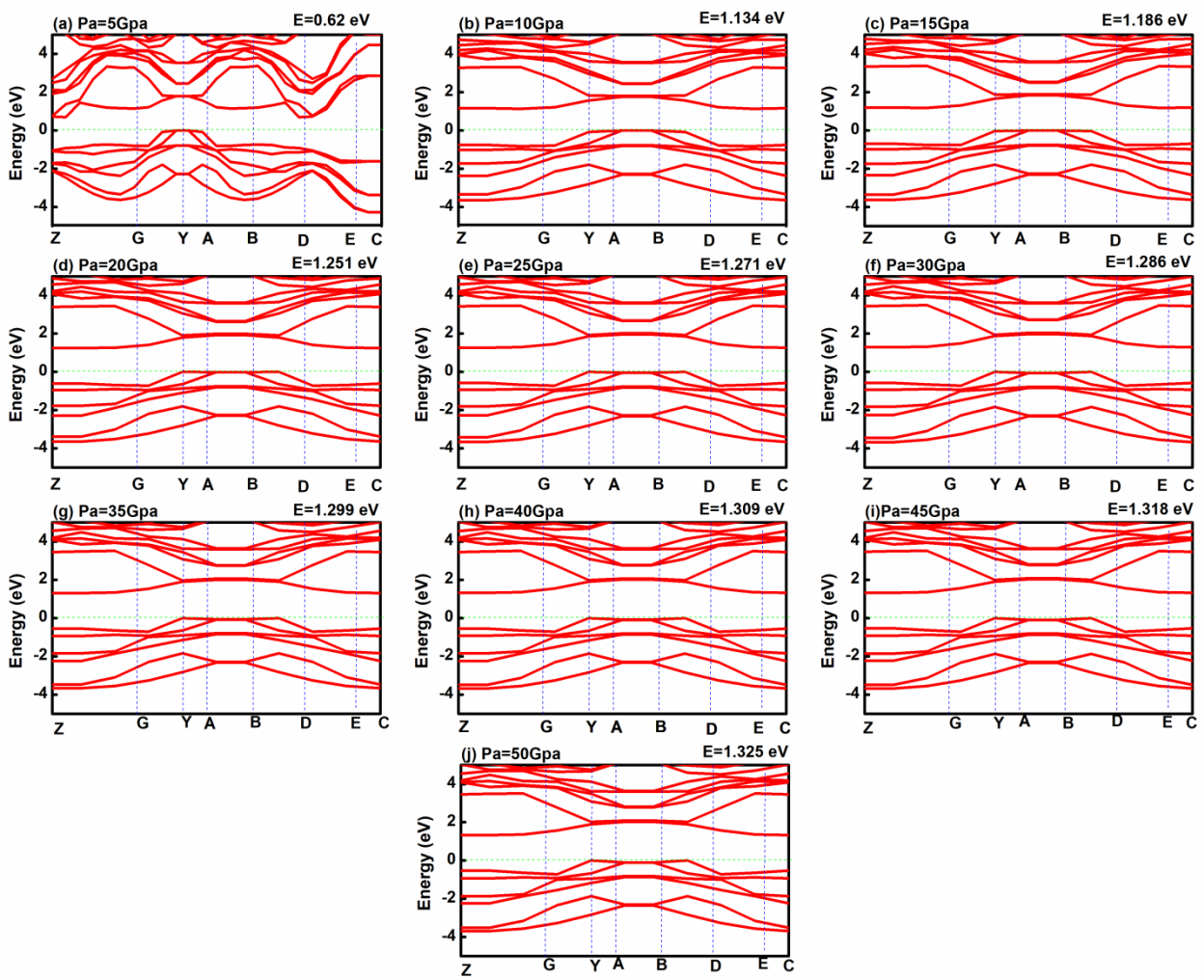

Figure 5: The calculated band structure of 2D-monochalcogenides PbSe under varying pressure from 0 to 50 GPa. Subfigures (a) through (j) correspond to the band structures at specific pressure points: (a) 0 GPa, (b) 5 GPa, (c) 10 GPa, (d) 15 GPa, (e) 20 GPa, (f) 25 GPa, (g) 30 GPa, (h) 35 GPa, (i) 40 GPa, and (j) 50 GPa. The progressive changes illustrate the pressure-induced modifications to the band gap and electronic dispersion, potentially indicating a topological phase transition or a direct-to-indirect band gap crossover. The Fermi level is set at 0 eV.

Additionally, pressure can weaken interlayer interactions in materials. When pressure weakens these interlayer interactions, it reduces the overlap of electronic wave function between the layers, leading to more isolated electronic state. This isolation increases the localization of electrons within each layer, which makes the energy level in conduction and valance band more distinct and ultimately enhancing the energy difference between the conduction and valence bands [36]. Furthermore, the application of increased pressure can introduce strain within the crystal lattice, disrupting atomic positions. Such disturbances may distort atomic orbitals and shift the band edge, consequently increasing the band gap as strain alters the electronic environment of the material. Pressure can also impact various crystallographic directions differently. Anisotropic compression can lead to non-uniform changes in the band gap, potentially resulting in an overall increase, as some directions may experience more compression and contribute more significantly to the electronic band structure than others.

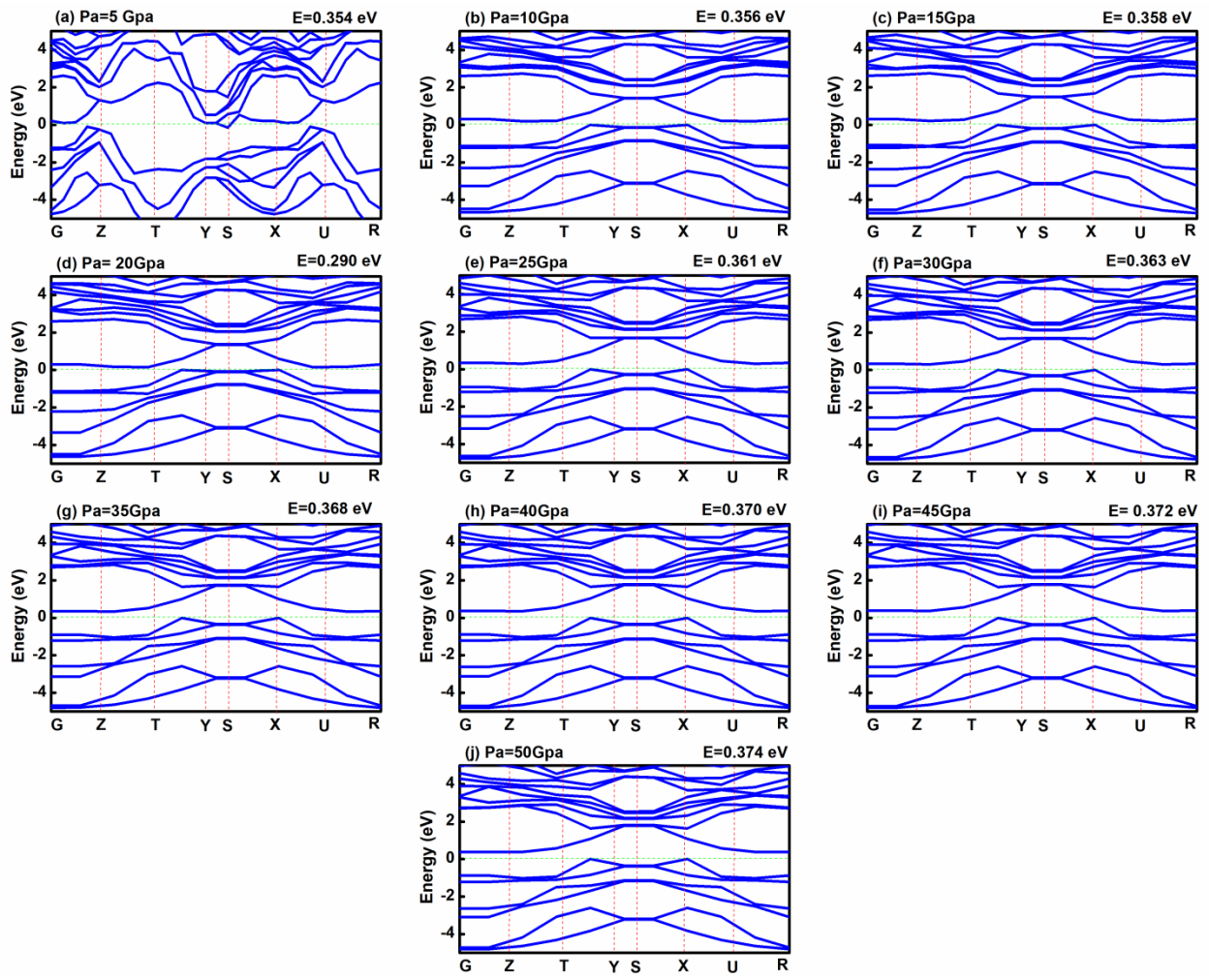

Figure 6: The calculated band structure of 2D-monochalcogenides PbTe under varying pressure from 0 to 50 GPa. Subfigures (a) through (j) correspond to the band structures at specific pressure points: (a) 0 GPa, (b) 5 GPa, (c) 10 GPa, (d) 15 GPa, (e) 20 GPa, (f) 25 GPa, (g) 30 GPa, (h) 35 GPa, (i) 40 GPa, and (j) 50 GPa. The progressive changes illustrate the pressure-induced modifications to the band gap and electronic dispersion, potentially indicating a topological phase transition or a direct-to-indirect band gap crossover. The Fermi level is set at 0 eV.

As the applied pressure increased from 0 to 50 GPa, the band gap of the material showed a noticeable rise from 0 eV to 0.374 eV as shown in Figure 6. This behavior is characteristic of semiconductors and semimetals, where the band gap typically increases in the initial stages of compression. Under higher pressure, the density of defect states within the band gap was significantly reduced, indicating that the material was driven toward a more ordered and stable configuration. Additionally, the number of electronic states near the Fermi level decreased, meaning fewer mid-gap states were available for electronic transitions. Overall, these combined effects, reduced defect density, fewer available electronic states, and the inherent semiconducting response to pressure, led to an effective widening of the band gap.

When a pressure of 20 GPa was applied, the band gap of the material decreased to 0.290 eV. This reduction was primarily attributed to a slight reconfiguration in the electronic structure caused by lattice compression. The applied pressure led to a decreased distance between Pb and Te atoms, which enhanced the orbital overlap due to their increased atomic proximity. As a result, the energy

separation between the conduction band (CB) and valence band (VB) was reduced, lowering the energy required for electron transitions. Overall, the combined effects of lattice compression and enhanced orbital overlap resulted in a noticeable contraction, or narrowing, of the band gap. In addition, the applied pressure fosters increased electron delocalization throughout the lattice, which diminishes the differences between energy levels and consequently reduces the band gap. As pressure increases, structural distortions arise that shift atomic positions and modify the bonding environment, thereby decreasing the band gap. Besides this, the application of pressure had a pronounced effect on the electronic structure of the material, primarily through its influence on atomic bonding and orbital interactions. Compression of the Pb–Te bond lengths intensified the interaction between bonding and anti-bonding states, thereby decreasing the energy difference between them and resulting in a lower band gap energy. Additionally, pressure-induced lattice distortions caused a downward shift in the conduction band minimum (CBM) and compressed the energy states near the band edges, which further reduced the energy separation between the conduction and valence bands. Enhanced Pb–Te orbital hybridization under pressure strengthened the interaction between the conduction band (CB) and valence band (VB), contributing to a further narrowing of the band gap. Moreover, the weakening of Ge–Te covalent bonds directly reduced the energy separation between bonding and anti-bonding states, reinforcing the overall trend of band gap narrowing with increasing pressure.

After the application of 20 GPa pressure, the band gap exhibited a gradual increase, indicating that the material began to recover after reaching its minimum value at this pressure, as shown in Fig. 5. Upon further compression, the band gap continued to increase due to structural adjustments within the material. These adjustments involved modifications in bond lengths and atomic arrangements, which contributed to the widening of the band gap. Overall, the observed trend highlights the material's ability to undergo electronic structure recovery through pressure-induced structural reconfiguration, as illustrated in Fig. 5.

So, these pressure-induced transitions arise from orbital hybridization, electron delocalization, and bond length variation, confirming that controlled compression can tune the semiconducting nature of Pb-chalcogenide monolayers. Among them, PbSe demonstrates an optimal balance between structural stability and electronic tunability, making it the most promising material for next-generation optoelectronic and photovoltaic applications under extreme conditions.

4 Conclusions

This study presents a comprehensive first-principles investigation of two-dimensional lead monochalcogenides PbX (X = S, Se, Te) using the CASTEP code within the GGA–PBE approximation. The puckered, buckled, and planar configurations were systematically modeled to examine the influence of atomic geometry and external pressure on stability and electronic properties. The optimized structures reveal that the puckered phase exhibits the greatest thermodynamic stability, with binding energies of −4.25 eV (PbS), −4.20 eV (PbSe), and −3.02 eV (PbTe), confirming their energetic favorability over the buckled and planar phases. The corresponding bond lengths follow the order PbS (2.54 Å) < PbSe (2.688 Å) < PbTe (3.22 Å), consistent with increasing atomic radius and lattice expansion. Phonon dispersion confirmed the dynamic stability of all structures through the absence of imaginary frequencies.Electronic structure analysis indicates indirect band gaps of 1.01 eV for PbS and 0.70 eV for PbSe, while PbTe exhibits metallic behavior at ambient conditions. Under hydrostatic compression up to 50 GPa, the band gap of PbS increases from 1.188 eV to 1.904 eV, and that of PbSe rises from 0.70 eV to 1.325 eV, demonstrating strong pressure-induced semiconducting enhancement. PbTe shows a non-monotonic response, with the gap decreasing to 0.290 eV at 20 GPa and recovering to 0.374 eV at 50 GPa, reflecting a semiconductor–semimetal transition driven by orbital hybridization and lattice rearrangement. Overall, the results confirm that structural anisotropy and external pressure play decisive roles in tuning the optoelectronic properties of 2D PbX systems. Among all, PbSe demonstrates the most balanced combination of structural stability and band gap

tunability, making it a promising candidate for high-efficiency optoelectronic and photovoltaic applications in high-pressure or extraterrestrial environments.

Acknowledgement: This research was supported by the Higher Education Commission of Pakistan through the National Research Programme for Universities-NRPU with research project No: No. 20-16683/NRPU/R&D/HEC/2021.

Funding Statement: This research was supported by the Higher Education Commission (HEC) of Pakistan under the National Research Programme for Universities (NRPU) [Project No. 20-16683/NRPU/R&D/HEC/2021]. The funders had no role in the study design, data collection and analysis, decision to publish, or preparation of the manuscript. No additional external funding was received for this work.

Author Contributions: Each co-author has made a unique contribution to this work. M. Tariq was responsible for writing – original draft, methodology, software, and investigation. R. Ahmed and S. A. Tahir were responsible for supervision, project administration, validation, and writing – review & editing. B. U. Haq contributed to writing – review & editing, formal analysis, and data curation. F. K. Butt was responsible for funding acquisition, resources, and conceptualization. M. W. Majeed contributed to data curation, and visualization. A. Hussain contributed to investigation, validation, and conceptualization

Availability of Data and Materials: The datasets generated and/or analyzed during the current study are available from the corresponding author, M. Tariq, upon reasonable request.

Ethics Approval: Not applicable. This research did not involve human participants or animals.

Conflicts of Interest: The authors declare that there are no conflicts of interest regarding the publication of this paper.

References

1. Bermudez-Garcia A, Voarino P, Raccurt O. Environments, needs and opportunities for future space photovoltaic power generation: a review. Appl Energy. 2021; 290:116757. http://doi.org/10.1016/j.apenergy.2021.116757.
2. Wilberforce T, Baroutaji A, El Hassan Z, Thompson J, Soudan B, Olabi AG. Prospects and challenges of concentrated solar photovoltaics and enhanced geothermal energy technologies. Sci Total Environ. 2019;659:851–61. http://doi.org/10.1016/j.scitotenv.2018.12.257.
3. Lawrence JD, Mullen AD, Bryson FE, Chivers CJ, Hanna AM, Plattner T, et al. Subsurface science and search for life in ocean worlds. Planet Sci J. 2023;4(2):22. http://doi.org/10.3847/psj/aca6ed.
4. Azarhoosh P, McKechnie S, Frost JM, Walsh A, van Schilfgaarde M. Research update: relativistic origin of slow electron-hole recombination in hybrid halide perovskite solar cells. APL Mater. 2016;4(9):091501. http://doi.org/10.1063/1.4955028.
5. Dittrich T. Materials concepts for solar cells. Singapore: World Scientific Publishing; 2018.
6. Al-Ezzi AS, Ansari MNM. Photovoltaic solar cells: a review. Appl Syst Innov. 2022; 5(4):67. http://doi.org/10.3390/asi5040067.
7. Machín A, Márquez F. Advancements in photovoltaic cell materials: silicon, organic, and perovskite solar cells. Materials. 2024;17(5):1165. http://doi.org/10.3390/ma17051165.
8. Viennois R, Niedziolka K, Jund P. Physical properties of the thermoelectric cubic lanthanum chalcogenides La3−yX4 (X = S, Se, Te) from first principles. Phys Rev B. 2013; 88(17):174302. http://doi.org/10.1103/physrevb.88.174302.
9. Caid M, Rached Y, Rached D, Cheref O, Rached H, Benalia S, et al. Electronic structure of short-period ZnSe/ZnTe superlattices based on DFT calculations. Condens Matter Phys. 2022;25(1):13701. http://doi.org/10.5488/cmp.25.13701.
10. Xu L, Yang M, Wang SJ, Feng YP. Electronic and optical properties of the monolayer group-IV monochalcogenides MX (M = Ge, Sn; X = S, Se, Te). Phys Rev B. 2017;95(23):235434.
11. Peng Q, Rehman J, Butt MK, Shafiee SA, Yang Z, Ouladsmane M, et al. Two-dimensional SnS and SnSe as hosts of K-ion storage: a first-principles prediction. J Phys Chem C. 2023;127(32):15730.
12. Dai Y, Zhang X, Cui Y, Li M, Luo Y, Jiang F, et al. Theoretical insights into strong intrinsic piezoelectricity of blue-phosphorus-like group-IV monochalcogenides. Nano Res. 2022;15(1):209.

13. Ye Y, Guo Q, Liu X, Liu C, Wang J, Liu Y, et al. Two-dimensional GeSe as an isostructural and isoelectronic analogue of phosphorene: sonication-assisted synthesis, chemical stability, and optical properties. Chem Mater. 2017;29(19):8361.
14. Islam MA, Sarkar DK, Shahinuzzaman M, Wahab YA, Khandaker MU, Tamam N, et al. Green synthesis of lead sulphide nanoparticles for high-efficiency perovskite solar cell applications. Nanomaterials. 2022;12(11):1933. http://doi.org/10.3390/nano12111933.
15. Ma W, Swisher SL, Ewers T, Engel J, Ferry VE, Atwater HA, et al. Photovoltaic performance of ultrasmall PbSe quantum dots. ACS Nano. 2011;5(10):8140.
16. Swartz CH, LeBlanc EG, Perkins C, McGott DL, Reese MO, Nichols A, et al. Evaluation of PbTe and SnTe as ohmic contact layers in CdTe solar cell devices. Appl Surf Sci. 2022; 598:153656. http://doi.org/10.1016/j.apsusc.2022.153656.
17. Gupta DC, Hamid I. Lead-chalcogenides under pressure: ab initio study. Int J Mod Phys Conf Ser.2013;22:612–8.
18. Öztürk H, Arslan GG, Kürkçü C, Yamçıçıer Ç. Structural phase transformation, intermediate states and electronic properties of PbTe under high pressure. J Electron Mater. 2020;49(5):3089–95.
19. Rached D, Rabah M, Benkhettou N, Driz M, Soudini B. Calculated band structures and optical properties of lead chalcogenides PbX (X = S, Se, Te) under hydrostatic pressure. Physica B 2003;337(1):394–403.
20. Sohrabikia Z, Abedi Ravan B, Jafari M. Tuning band gaps in lead chalcogenides under pressure: implications for infrared detection applications. Phys Scr. 2024; 99(7):075975. http://doi.org/10.1088/1402-4896/ad551f.
21. Boukhris N, Meradji H, Korba SA, Drablia S, Ghemid S, El Haj Hassan F. First principles calculations of structural, electronic and thermal properties of lead chalcogenides PbS, PbSe and PbTe compounds. Bull Mater Sci. 2014;37(5):1159–66. http://doi.org/10.1007/s12034-014-0057-7.
22. Haq BU, AlFaify S, Alshahrani T, Ahmed R, Mahmood Q, Tahir SA, et al. Exploring the potential of lead-chalcogenide monolayers for room-temperature thermoelectric applications. Ceram Int. 2021:47(3);3380.
23. Nayak AP, Bhattacharyya S, Zhu J, Liu J, Wu X, Pandey T, et al. Pressure-induced semiconducting to metallic transition in multilayered molybdenum disulphide. Nat Commun. 2014;5(1):3734.
24. Islam MAU, Das O, Khadka DB, Islam MR, Rahman MF, Kato S, et al. Effect of low to high pressure on the structural, mechanical, electrical, and optical properties of inorganic material Ca_3AsBr_3: an ab initio investigation. ACS Omega. 2024;9(7):8005.
25. Shen P, Ma X, Guan Z, Li Q, Zhang H, Liu R, et al. Linear tunability of the band gap and two-dimensional (2D) to three-dimensional (3D) isostructural transition in WSe_2 under high pressure. J Phys Chem C. 2017;121(46):26019.
26. Tariq M, Shaari A, Chaudhary K, Jalil A, Dyana Ismail F, Ahmed R, et al. A DFT study on the switching energy of multiferroic capacitor with stable single-phase multiferroic material. Mater Sci Eng B. 2024;300:117070. http://doi.org/10.1016/j.mseb.2023.117070.
27. Tariq M, Shaari A, Chaudhary K, Ahmed R, Jalil MA, Ismail FD. Magnetoelectric, and dielectric based switching properties of Co-doped BiFeO3 for low energy memory technology: a first-principles study. Phys B Condens Matter. 2023;650:414489. http://doi.org/10.1016/j.physb.2022.414489.
28. Tariq M, Shaari A, Chaudhary K, Ahmed R, Jalil MA, Ismail FD. Computational study of switching properties in Mn and transition metal Co-doped BFO. Phys B Condens Matter. 2023; 652:414650. http://doi.org/10.1016/j.physb.2023.414650.
29. Tariq M, Chaudhary K, Shaari A, Jalil A, Ismail FD, Ahmed R, et al. Ultralow energy switching with spin polarized magneto-electric properties of co-doped cubic phase BFO: a first-principles study. Chin J Phys. 2022;79(1):211–24.
30. Tariq M, Shaari A, Chaudhary K, Ahmed R, Ismail FD. Exploring spin current and dielectric switching characteristics of doped-multiferroic in hexagonal phase for advance RAM technology: a theoretical study. Phys B Condens Matter. 2024; 691:416326. http://doi.org/10.1016/j.physb.2024.416326.
31. Kamal, C., Aparna Chakrabarti, and Motohiko Ezawa. "Direct band gaps in group IV-VI monolayer materials: Binary counterparts of phosphorene." Physical Review B 93, no. 12 (2016): 125428. doi: 10.1103/PhysRevB.93.125428
32. Hu, Ting, and Jinming Dong. "Two new phases of monolayer group-IV monochalcogenides and their piezoelectric properties." Physical Chemistry Chemical Physics 18, no. 47 (2016): 32514-32520. doi: 10.1039/c6cp06734d.

33. Ul Haq, Bakhtiar, S. AlFaify, R. Ahmed, Faheem K. Butt, A. Laref, and Mohd Shkir. "Exploring single-layered SnSe honeycomb polymorphs for optoelectronic and photovoltaic applications." Physical Review B 97, no. 7 (2018): 075438, doi: 10.1103/PhysRevB.97.075438
34. Gillani SSA, Ahmad R, Zeba I, Islah-u-din, Shakil M, Rizwan M, et al. Effect of external pressure on the structural stability, electronic structure, band gap engineering and optical properties of LiNbO3: an ab-initio calculation. Mater Today Commun. 2020;23:100919. http://doi.org/10.1016/j.mtcomm.2020.100919.
35. Gillani SSA, Zeeshan T, Maqsood A, Shakil M, Rizwan M, Ahmad R, et al. A systematic computational study to understand the effect of metals (Mg, Ca, Sr) doping and external isotropic static pressure on phase stability, electronic band structure and optical properties of KNbO3. Mater Sci Eng B. 2021;271:115261. http://doi.org/10.1016/j.mseb.2021.115261.
36. Miao M, Sun Y, Zurek E, Lin H. Chemistry under high pressure. Nat Rev Chem. 2020;4(10):508–27. http://doi.org/10.1038/s41570-020-0213-0.